Vesicles carry most exocyst subunits to exocytic sites marked by the remaining two subunits, Sec3p and Exo70p

Charles Boyd,[1] Thom Hughes,[2] Marc Pypaert,[1] and Peter Novick[1]

[1]Department of Cell Biology, Yale University School of Medicine, New Haven, CT 06520
[2]Department of Cell Biology and Neuroscience, Montana State University, Bozeman, MT 59717

Exocytosis in the budding yeast *Saccharomyces cerevisiae* occurs at discrete domains of the plasma membrane. The protein complex that tethers incoming vesicles to sites of secretion is known as the exocyst. We have used photobleaching recovery experiments to characterize the dynamic behavior of the eight subunits that make up the exocyst. One subset (Sec5p, Sec6p, Sec8p, Sec10p, Sec15p, and Exo84p) exhibits mobility similar to that of the vesicle-bound Rab family protein Sec4p, whereas Sec3p and Exo70p exhibit substantially more stability. Disruption of actin assembly abolishes the ability of the first subset of subunits to recover after photobleaching, whereas Sec3p and Exo70p are resistant. Immunogold electron microscopy and epifluorescence video microscopy indicate that all exocyst subunits, except for Sec3p, are associated with secretory vesicles as they arrive at exocytic sites. Assembly of the exocyst occurs when the first subset of subunits, delivered on vesicles, joins Sec3p and Exo70p on the plasma membrane. Exocyst assembly serves to both target and tether vesicles to sites of exocytosis.

Introduction

Cell polarity in eukaryotes is maintained in part by targeted delivery of vesicles to distinct regions of the plasma membrane (Drubin and Nelson, 1996; Nelson and Yeaman, 2001). Delivery of vesicles to their target membranes requires recognition between the vesicle and target membrane before fusion, and large multisubunit tethering complexes are thought to provide this initial recognition (Whyte and Munro, 2002). Tethering complexes have been identified that mediate vesicular transport to various compartments, including the Golgi apparatus (Sacher et al., 1998; Conboy and Cyert, 2000), the vacuole in yeast (Rieder and Emr, 1997), endosomes (Simonsen et al., 1998; Kim et al., 1999), and regions within the plasma membrane (TerBush et al., 1996). Secretory vesicles are tethered to the yeast plasma membrane by a multiprotein complex known as the exocyst. Eight subunits (Sec3p, Sec5p, Sec6p, Sec8p, Sec10p, Sec15p, Exo70p, and Exo84p) constitute the assembled exocyst (Guo et al., 1999a), and homologues of each of these proteins have been identified in diverse systems including plants (Elias et al., 2003), insects (Andrews et al., 2002; Murthy et al., 2003), and mammals (Hsu et al., 1996, 1998).

The exocyst was first purified from yeast by coimmunoprecipitation using an epitope-tagged allele of Sec8p (TerBush et al., 1996). All members of the exocyst except Sec3p are essential for viability, whereas loss of Sec3p results in slow growth and decreased spatial control of exocytosis at 25°C and inhibition of both growth and secretion at 37°C (Bowser and Novick, 1991; TerBush and Novick, 1995; Guo et al., 1999a; Wiederkehr et al., 2003). The exocyst displays a characteristic, cell cycle–dependent localization pattern that begins with the appearance of a small cap at sites of bud formation. This cap persists at the apical tip of the growing bud until the time of nuclear division when it shifts to an isotropic distribution over the surface of the growing bud. Finally, there is an abrupt shift in localization to the mother-bud neck near the time of cytokinesis, where it remains until cell separation (TerBush and Novick, 1995, Finger et al., 1998). This pattern of localization mirrors the pattern of deposition of newly synthesized material at the cell surface (Field and Schekman, 1980).

Although all exocyst subunits share the same pattern of localization, they exhibit strikingly different requirements for this localization. The polarized localization of Sec3p is insensitive to blocks in membrane traffic as well as to disruption of the actin cytoskeleton (Finger et al., 1998). Rather, its localization involves a direct interaction with the Rho family GTPases,

The online version of this article includes supplemental material.

Correspondence to Peter Novick: peter.novick@yale.edu

The Journal of Cell Biology, Vol. 167, No. 5, December 6, 2004 889–901
http://www.jcb.org/cgi/doi/10.1083/jcb.200408124

Rho1p and Cdc42p, in their GTP-bound form on the plasma membrane (Drgonova et al., 1999; Guo et al., 2001; Zhang et al., 2001). In contrast, Sec8p requires both ongoing membrane traffic as well as actin function for its localization (Ayscough et al., 1997; Finger et al., 1998). Sec15p, a direct effector of the Rab GTPase Sec4p (Guo et al., 1999b), was found, like Sec4p, to associate with secretory vesicles, at least upon overexpression. Based on these observations, we have proposed that Sec3p serves as a spatial landmark on the plasma membrane for incoming secretory vesicles (Finger et al., 1998). Other subunits, we speculated, either ride the vesicles to these sites or are recruited to the sites directly from the cytosol in response to the arrival of the secretory vesicles. Assembly of the complex would then occur as vesicles arrive at the sites marked by Sec3p and would serve to tether the vesicles to the plasma membrane at these sites. In support of the model, we have shown that in a *sec4-8* mutant, in which vesicle delivery is blocked, a pool of Sec3p develops that sediments more slowly than the fully assembled exocyst complex (Guo et al., 2001).

Several lines of evidence from mammalian epithelial and neuronal cell lines also contribute to a model in which exocyst subunits arrive at sites of exocytosis on vesicles. In rat brain lysates (Brymora et al., 2001) and in PC12 neuronal cell lysates (Moskalenko et al., 2002, 2003), the Sec5 and Exo84 subunits of the mammalian exocyst have been found to associate with RalA, which in turn is found on synaptic and axonal vesicles (Bielinski et al., 1993). Elements of the exocyst have also been found associated with other compartments in the secretory pathway, including the endoplasmic reticulum in MDCK cells (Grindstaff et al., 1998), the trans-Golgi network of NRK cell lysates (Yeaman et al., 2001), vesicles in PC12 cell and rat brain lysates (Moskalenko et al., 2002; Sans et al., 2003), and complexed with GTP-bound ARF6 on endosomes found in MDCK and NRK cell lysates (Prigent et al., 2003).

The detailed mechanism by which the exocyst functions in tethering is under investigation. Central to this question is how the exocyst comes to be assembled at exocytic sites. Related to this issue is the dynamic behavior of the exocyst subunits, and how the behavior of individual exocyst subunits bears on the mechanism of tethering at a molecular level. Here, we systematically examine the dynamic behavior, in live yeast cells, of each of the exocyst subunits fused to GFP by photobleaching recovery experiments. We have also used immunogold electron microscopy and video fluorescence microscopy to show that a subset of exocyst subunits is transported on vesicles to sites of exocytosis at the plasma membrane where they assemble with the remaining subunits.

Results

FRAP analysis reveals two classes of exocyst components

We conducted FRAP experiments on strains expressing exocyst proteins fused at their carboxy termini to GFP. In addition, a strain expressing Sec4p fused at its amino terminus to GFP was also examined. The constructs were expressed at normal levels and as the sole copy. None of the strains exhibited any adverse effects on growth characteristics in either YPD or SC media, and all fusion proteins showed localization patterns identical to the patterns determined by immunofluorescence of c-myc– or HA-tagged exocyst proteins (TerBush and Novick, 1995): at incipient bud sites, in a cap in small buds that shifted to an isotropic distribution over the surface of large buds, and at the mother/bud neck near the time of cytokinesis.

We photobleached bud tips with a fixed dye-tunable laser emitting light at a wavelength of 440 nm, focused to a small spot $\sim$1 μm in diameter. The absorption peak of GFP is 489 nm, but absorption extends far enough into the blue to allow the 440-nm laser to bleach GFP. Each bud tip was exposed to $\sim$10 pulses of 50 μs duration, for a total bleaching time of 0.5 ms. We observed recovery by collecting standard epifluorescence images at $\sim$10-s intervals for 1–3 min, depending on which exocyst subunit was being observed (Fig. 1). For each time point, we measured fluorescence intensity in the bud tip and calculated the time constant τ for each subunit by plotting the natural logarithm of the left side of Eq. 2 (see Materials and methods) against time. This plot should have a single straight line if there is only one component to the recovery, but a discontinuous line with two distinct slopes if there are two components that contribute to recovery. In these plots the slope(s) of each line is equal to $-1/\tau$. For each subunit, at least 12 lines were generated using IGOR and used to calculate an average τ. All subunits except Exo70-GFP exhibited single-time constant kinetics (Fig. 2 A), whereas Exo70-GFP exhibited a recovery characterized by two modes of recovery, with τ of 22 $\pm$ 9 s for the fast mode and 57 $\pm$ 17 s for the slow mode. The overall rate of Exo70p-GFP recovery was 41 $\pm$ 13 s, implying that $\sim$46% of Exo70p-GFP recovers via the fast mode of recovery, whereas the remaining 54% uses the slow mode.

Fig. 2 B is a chart comparing the time constants of all the recoveries measured, including both the fast and slow recovery modes of Exo70p-GFP. The τ values fall into two general categories: long recovery times of $\sim$1 min duration (Sec3p-GFP and the slow mode of Exo70p-GFP recovery), and shorter recovery times for the remainder of the exocyst subunit fusions, the fast mode of Exo70-GFP recovery, and GFP-Sec4p. Sec4p is anchored to secretory vesicles by a COOH-terminal geranylgeranyl tail (Goud et al., 1988), so we used an amino-terminal GFP-Sec4p fusion as a proxy measurement for vesicle movement to the bud tip. The recovery τ for GFP-Sec4p is $\sim$12 s. When we measured recovery τ for exocyst subunits, we found that most of them (the exceptions being Sec3p-GFP and the slow mode of Exo70p-GFP) recovered from photobleaching at approximately the same rate as GFP-Sec4p.

We found no evidence to support the existence of an immobile fraction of exocyst subunits at sites of exocytosis. Recovery efficiency of photobleached tips depends on the fraction of the total cellular signal bleached. In all cases, the recovery efficiency measured was approximately equal to the expected recovery efficiency as determined by measuring the fraction of total signal bleached.

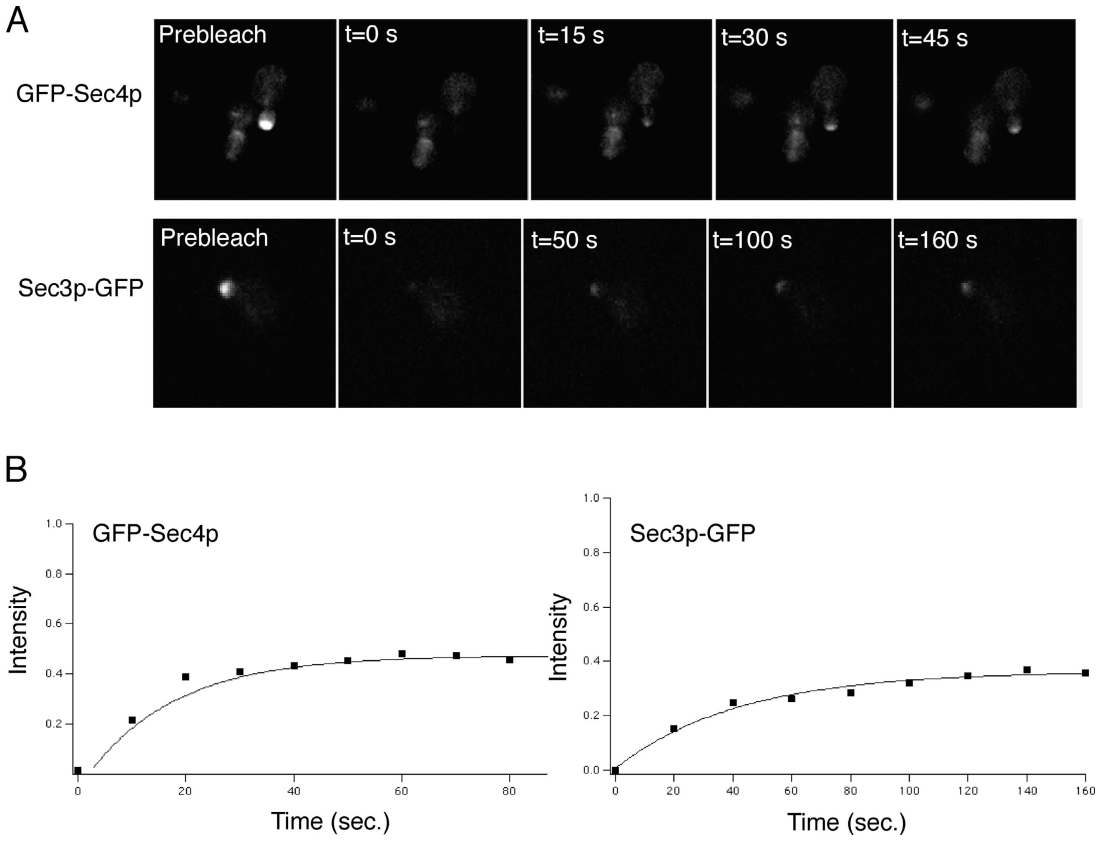

Figure 1. **Fluorescence recovery of GFP-tagged exocyst subunits in *S. cerevisiae*.** Haploid cells with integrated GFP fusion genes in an otherwise wild-type background were grown in SC medium at 25°C and mounted as described in Materials and methods. Bud tips were bleached with a fixed dye-tunable laser emitting at a wavelength of 440 nm, and images were recorded for analysis at various time points. (A) Two time series of recovery from photobleaching. GFP-Sec4p recovers completely in 45 s with a τ of 12 $\pm$ 4 s, whereas Sec3p-GFP requires about 3 min to recover completely, with a τ of 59 $\pm$ 17 s. Recovery is limited to $\sim$35% because approximately two-thirds of each exocyst subunit is located in the bud tip at any given time. (B) Best-fit recovery curve determination for the recoveries of GFP-Sec4p and Sec3p-GFP in part A. IGOR was used to generate a value for τ and to plot a recovery curve for each recovery experiment.

FRAP in the presence of Latrunculin A indicates that recovery of one class depends on the actin cytoskeleton

Because the recovery times for those subunits that appeared to use the fast mode of recovery were more similar to the recovery time for GFP-Sec4p than the recovery times for Sec3p-GFP or the slow mode for Exo70p-GFP, we decided to investigate whether or not all of the fast-recovering group used the same mechanism of recovery as GFP-Sec4p. Because GFP-Sec4p is present on vesicles that are transported to the bud tip along actin cables, we decided to test if recovery from photobleaching for all exocyst subunits depends on the presence of an intact actin cytoskeleton. As one test of this hypothesis, we treated cells with the actin-depolymerizing agent Latrunculin A. At a concentration of 200 μM, Latrunculin A treatment abolishes actin-based structures within 5 min in yeast (Ayscough et al., 1997). Vesicle transport to the bud tip halts, as shown by the effect on GFP-Sec4p localization, which showed a time-dependent loss of GFP-Sec4p from the bud tip (unpublished data). We examined by FRAP the population of cells that had not yet lost a focus of localized GFP in the time frame from 5 to 30 min after addition of Latrunculin A. We found that recovery of exocyst-GFP fusions was substantially inhibited (Fig. 3). In most cases there was only a small amount of recovery observed, <5%, but based on this low efficiency and the speed of this fraction's recovery (complete within 10 s), it may represent a freely diffusible population of each subunit, though we have no information on the size of this population in Latrunculin A–treated cells. Because we observed little recovery from photobleaching in the presence of Latrunculin A during the 5 to 30 min window after Latrunculin A addition, our conclusion is that delivery of these exocyst subunits to the bud tip depends on actin.

However, under the same conditions of Latrunculin treatment, Sec3p-GFP remained stably located at the bud tip, as previously noted (Finger et al., 1998), and indeed we measured no loss of Sec3p-GFP photobleaching recovery efficiency and no significant change in the recovery τ in the presence of Latrunculin A (Fig. 3). In the presence of Latrunculin A, Exo70p-GFP showed a linear recovery profile that was characteristic of a single mode of recovery (Fig. 3 D), and the rate of recovery matched the rate of the slow mode of recovery that we had calculated based on the slope of the Exo70p-GFP recovery plot in untreated cells.

Two results from the FRAP analysis stand out in significance: first, in the case of all fusions except Sec3p-GFP and Exo70p-GFP, an assembled actin network is necessary to recover

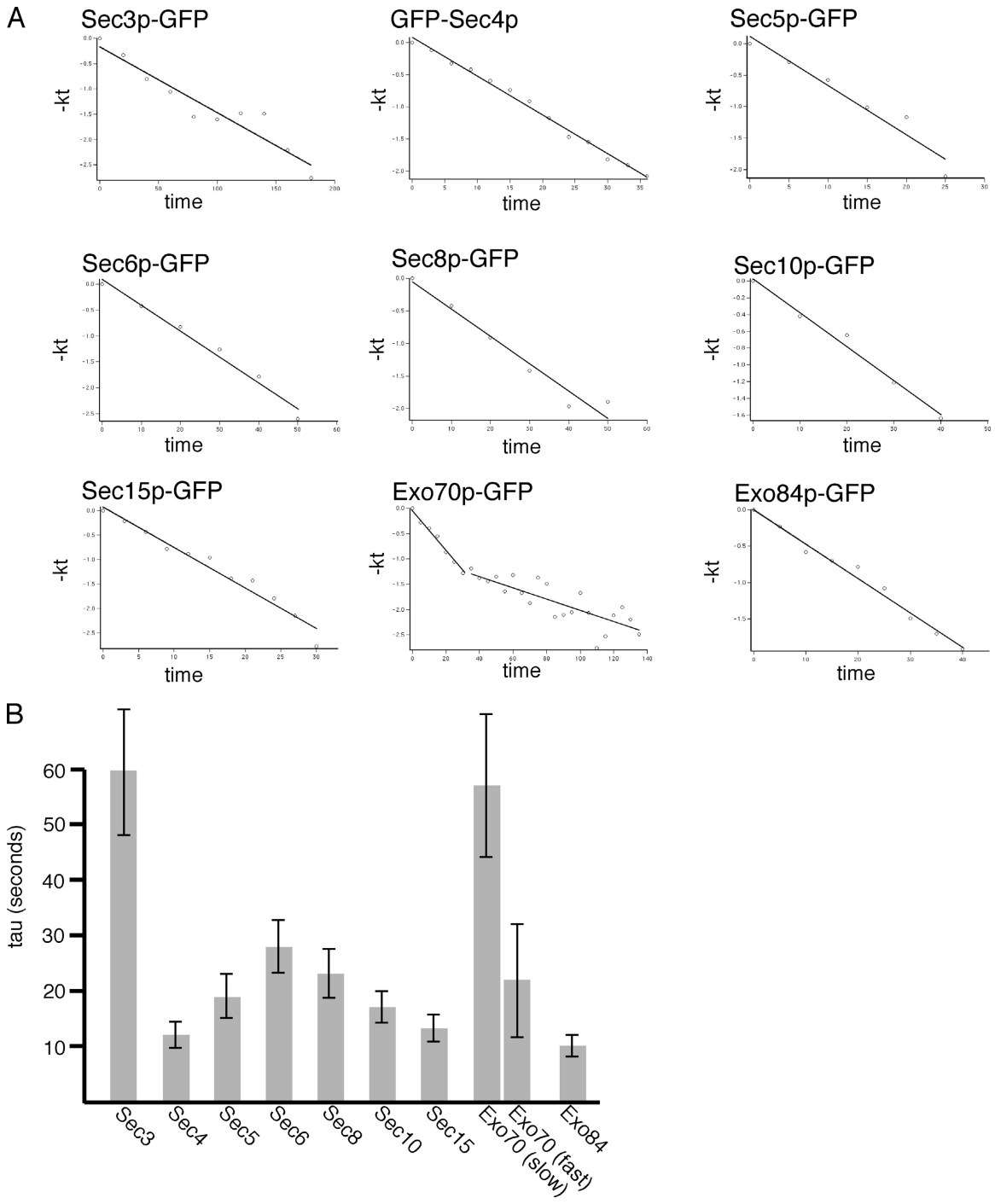

Figure 2. **Determination of kinetic components of recovery.** Recovery from photobleaching is described by Eq. 1 (see Materials and methods): $I_\infty - I_t = (I_\infty - I_0)e^{-kt}$, where I_∞ is the signal intensity at full recovery, I_t is the signal intensity at time t, I_0 is the signal intensity immediately after photobleaching, k is the rate constant (equivalent to $-1/\tau$), and t is time. (A) Plot of kt versus time will be characterized by a single line if recovery has one component or segments with two different slopes if recovery has two components. All exocyst components except Exo70p-GFP show a fit to a single line. Exo70p-GFP has two segments with differing slopes, indicating that there are two modes of photobleaching recovery for this subunit. (B) Histogram comparing FRAP recovery times for exocyst subunits and GFP-Sec4p. For each subunit, a best-fit curve determination was made for each photobleaching experiment, and the average τ of 12 recovery curves was calculated. In the case of Exo70p-GFP, both the fast and slow components are shown. Error bars represent 95% confidence intervals.

from photobleaching; second, those subunits that are dependent on actin normally have a recovery time that is more similar to that of the GFP-Sec4 fusion protein than to the actin-independent subunit Sec3p-GFP or the slow mode of Exo70p-GFP recovery. Both of these results are consistent with the hypothesis that six of the eight exocyst subunits (and approximately half of Exo70p-GFP) are delivered to sites of exocytosis on secretory vesicles. We further tested this hypothesis by two methods: first, we ascertained the distribution of the exocyst subunits using immunogold electron microscopy and correlated that distribution with the presence of vesicular structures; second, we imaged the movement of exocyst-GFP fusion proteins in live cells.

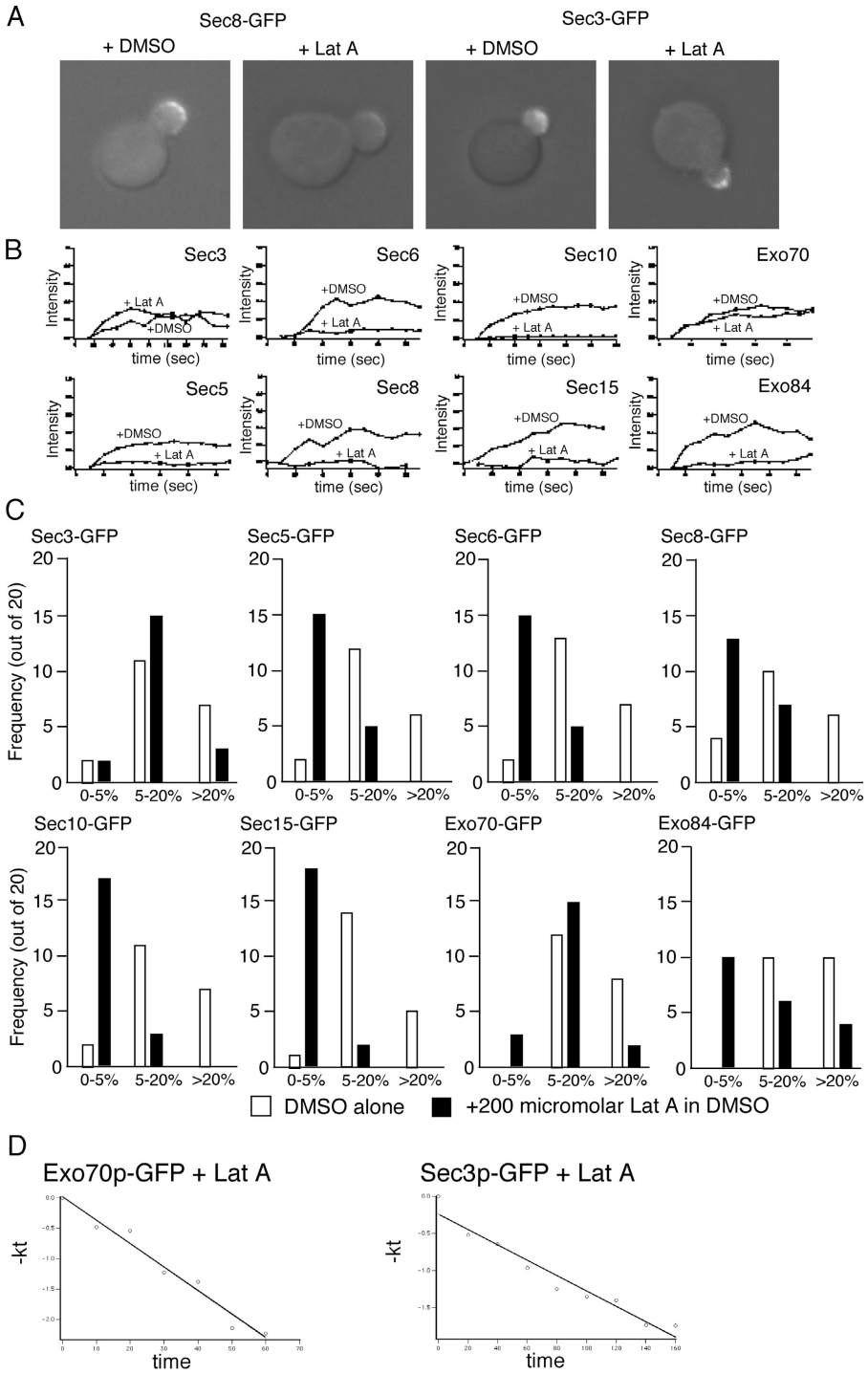

Figure 3. **Photobleaching recovery of GFP-tagged exocyst subunits in the presence of Latrunculin A.** Cells were grown in SC medium and prepared as described in Materials and methods. (A) Micrographs of strains containing Sec8-GFP and Sec3-GFP (NY2442 and NY2439, respectively) in cells with or without 200 mM Latrunculin A added to the medium. (B) Bud tips in Latrunculin A–treated cells were bleached and monitored for recovery. Sample recovery graphs with DMSO and DMSO + 200 μM Latrunculin A are shown for each exocyst subunit fused to GFP. (C) 20 bleach/recovery procedures for each of the GFP fusion strains were performed, and the frequencies of good (>20%), medium (5 to 20%), or poor (<5%) recovery with and without Latrunculin A present were plotted. (D) In the presence of Latrunculin A, both Sec3p-GFP and Exo70p-GFP displayed recovery kinetics characterized by a single mode of recovery. Sec3p-GFP had a recovery τ of 59 $\pm$ 11 s, whereas Exo70p-GFP had a recovery τ of 57 $\pm$ 13 s.

Electron microscopy reveals association of vesicles with exocyst proteins

To use immunoelectron microscopy confidently to assess the association of exocyst proteins with secretory vesicles, we needed both a negative and positive control. As a negative control, we looked for a protein that is concentrated at bud tips, but is not associated with vesicles. Spa2p helps to maintain the polarization of actin cables by facilitating the localization of the formin Bni1p (Fujiwara et al., 1998). Because the localization of Spa2p to the bud tip is known to be independent of actin (Ayscough et al., 1997), we would not expect it to be delivered on secretory vesicles. As a positive control we chose Sec2p, the exchange factor for Sec4p, because it has been shown to be associated with secretory vesicles (Walch-Solimena et al., 1997). Sec4p itself was not used as a positive control for two reasons. First, the 13myc-Sec4p fusion protein was not fully functional, and when present as the sole copy of Sec4p in the cell caused buildup of unfused vesicles (unpublished data). Second, although Sec4p maintains its membrane association with a carboxy terminal lipid anchor,

Table I. **Immunoelectron microscopy**

Fusion	Number of cells counted	Number of gold particles	Number of vesicles
None	35	1588	422
Spa2p-13myc	15	534	161
Sec2p-13myc	16	665	184
Sec3p-13myc	41	718	580
Sec5p-13myc	16	312	163
Sec6-13myc	36	2071	589
Sec8-13myc	34	1895	408
Sec10p-13myc	31	575	569
Sec15p-13myc	33	734	558
Exo70p-13myc	27	318	377
Exo84p-13myc	22	1492	196

Sec2p, as a peripheral membrane protein, is more similar to the exocyst proteins. Spa2p, Sec2p, and all eight exocyst subunits were tagged at their carboxy termini with 13 myc epitopes. Table I shows the numbers of gold particles, cells, and vesicles counted as part of the experiment for each fusion protein examined.

Fig. 4 shows that Spa2p-13myc is concentrated at the bud tip near the plasma membrane, but is not associated with vesicles. For the exocyst subunits and Sec2-13myc, we determined the density of gold particle labeling on vesicles versus the remainder of the cell, including the plasma membrane, to determine if there was a significant increase in labeling near vesicles. In contrast to Spa2p, an association of gold particles with vesicles was observed for Sec2p-13myc and all exocyst subunits with the exception of Sec3p-13myc. Fig. 4 also shows the differences in label density, expressed as the ratio of labeling in the cell as a whole to labeling near vesicles (see Materials and methods). For the untagged, wild-type control strain, this ratio should be unity because random background labeling should have no bias toward or against vesicles, and this is in fact what was observed. Other strains expressing various exocyst subunits fused to 13myc tags showed a range of labeling ratios, from approximately two- to fourfold above background levels. The conclusion we draw from this experiment is that all exocyst subunits, except for Sec3p, are associated with vesicles in transit to sites of exocytosis.

We also calculated the average distance in the bud tips from the plasma membrane to Spa2p-13myc, Sec3p-13myc, and Sec15p-13myc (as an exemplar of the exocyst subunits other than Sec3p). The results are plotted in Fig. 5. The average distance of gold particles from the plasma membrane for Spa2p-13myc and Sec3p-13myc are quite similar, indicating that Sec3p-13myc is associated with the membrane. In contrast, Sec15p-13myc is on average twice as distant from the plasma membrane as Spa2p-13myc. Histograms showing the distribution of each set of gold particles are also shown in Fig. 5. These data show that the distribution of Sec3p-13myc more closely resembles that of Spa2p-13myc rather than Sec15p-13myc, again indicating that the localization of Sec3p-13myc is more similar to that of Spa2p than Sec15p. The broader distribution of gold particles associated with Sec15p-13myc presumably reflects that some particles are found in the middle regions of bud tips as they are transported on vesicles to sites of exocytosis.

Video microscopy of strains harboring GFP fusion proteins

We reasoned that if exocyst subunits associate with vesicles before their arrival at the bud tip, it might be possible to capture video sequences of vesicles bearing GFP-tagged subunits in transit to sites of exocytosis. Previous reports have shown that this is possible with a GFP-Sec4p fusion protein, when it is overexpressed (Schott et al., 2002), so we reasoned that with improvements in camera technology it might be possible for exocyst subunits as well, even under conditions in which they are expressed at wild-type levels, which is thought to be from several hundred to a thousand copies per cell (Ghaemmaghami et al., 2003). However, we found that triple-GFP tags were necessary to boost the signal level from fluorescent fusions, other than GFP-Sec4p, to reliably capture movies of vesicles in motion. In strains harboring triple-GFP–tagged exocyst fusion proteins, we observed small puncta of fluorescence moving in a manner consistent with secretory vesicles. The average rates of puncta movement for each fusion protein are tabulated in Fig. 6 A; they are all nearly equal to the movement rate of an overexpressed GFP-Sec4p fusion protein as previously reported (Schott et al., 2002). Fig. 6 B shows several stills from a movie of a Sec5p-GFP fusion construct in an otherwise wild-type cell. A Quicktime movie of the complete sequence, as well as movies of the other exocyst-3xGFP fusion proteins in wild-type cells, is available in the online supplemental material (available at http://www.jcb.org/cgi/content/full/jcb.200408124/DC1).

The *sec4-8* allele slows recovery from photobleaching

To verify that FRAP analysis can measure nonactin-mediated perturbations of the secretory system, we tested the effect of a temperature-sensitive *sec4* mutation on the photobleach recovery rate of a Sec8p-GFP fusion. In a wild-type background, Sec8p-GFP recovers with a τ of $\sim$20 s, but when the Sec8p-GFP recovery rate was measured in a strain harboring the *sec4-8* allele the result was quite different. This *sec4* allele (G147D) has a reduced affinity for GTP, grows more slowly than wild-type at permissive temperatures, and is lethal at the restrictive temperature (Walworth et al., 1989). Fig. 7 A shows that at the permissive temperature we recorded a bleaching recovery rate for Sec8p-GFP of $\tau = 56 \pm 14$ s. No measurement at the restrictive temperature of the recovery rate of the Sec8p-GFP fusion was possible due to complications from heat shock and because bud tip localization of the Sec8p-GFP fusion was too infrequent at the restrictive temperature to bleach a representative sample. To test whether or not Sec4p function might be the rate-limiting step in recovery from photobleaching, we overexpressed Sec4p by a factor of 5–10-fold (Fig. 7 B). Under these conditions, there was no change from wild type in the rate of Sec8p-GFP recovery, indicating that under these conditions Sec4p is not the rate-limiting factor in the photobleaching recovery rate.

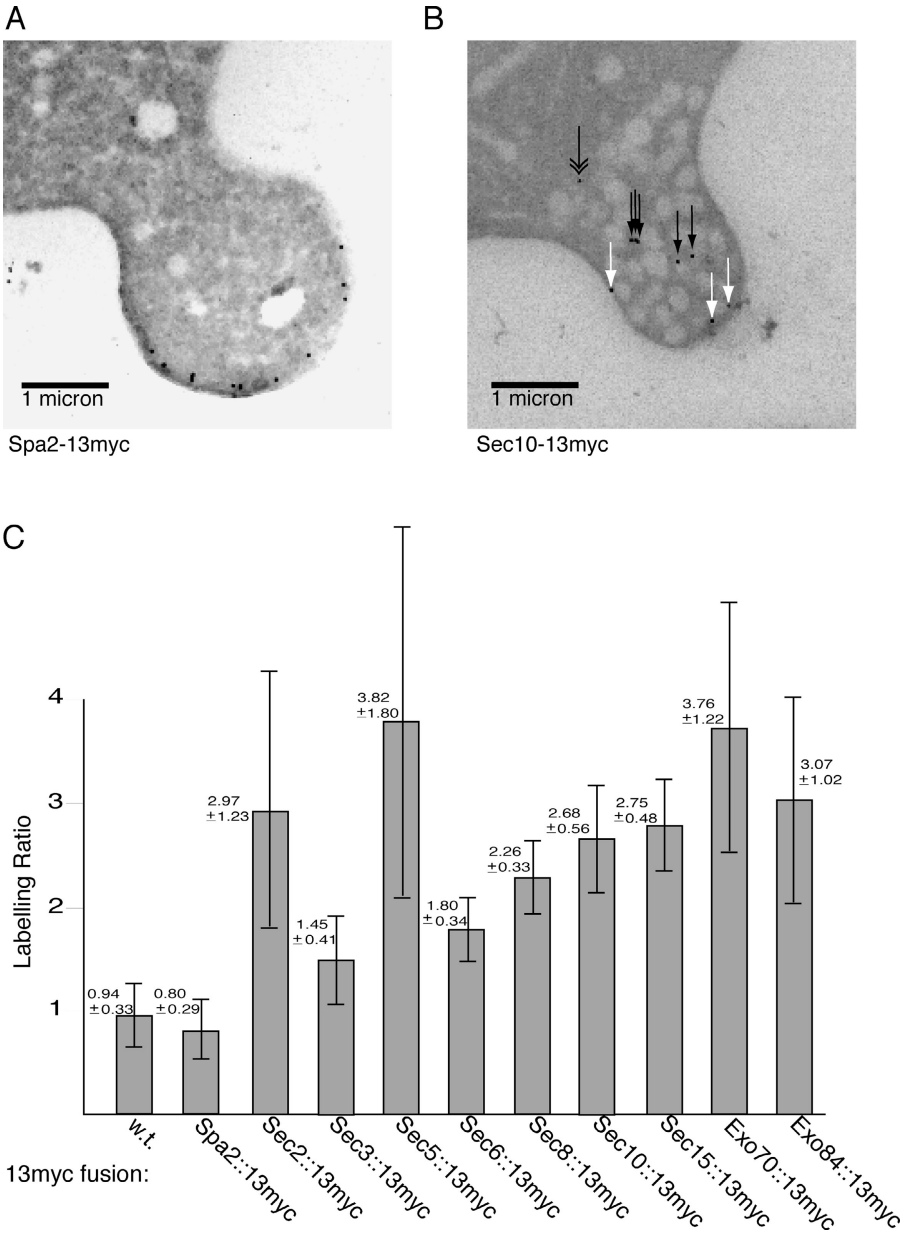

Figure 4. **Immunoelectron microscopy of 13myc-tagged exocyst subunits.** Haploid cells containing 13myc tags were grown in SC medium and cryosectioned as described in Materials and methods. (A) Immunoelectron micrograph of strain NY2508, which contains Spa2p fused to 13 consecutive 9E10 epitope tags in tandem. Fixed cryosections were labeled with anti-9E10 rabbit polyclonal antibody and 10-nm gold particles conjugated to protein A. (B) Immunoelectron micrograph of strain NY2504, which contains Sec10p fused to the 13myc epitope. The graph shows a tip with several vesicles visible at some distance from the plasma membrane. Gold particles associated with these vesicles are indicated by solid black arrows. Gold particles that are near both the plasma membrane and a vesicle are denoted by a white arrow, and gold particles that are not associated with any vesicle are denoted by the double arrows. (C) Histogram displaying the statistical significance of the association of gold particles with vesicles. Statistical significance was established by determining the surface areas of the cell and vesicles, counting gold particles, and then calculating the ratio of gold particle densities in each area; this factor is termed the labeling ratio (see Materials and methods). A labeling ratio of one indicates no association with vesicles, whereas a ratio >1 indicates colocalization of vesicles and gold particles, and indicates that exocyst subunits are associated with vesicles. Error bars represent 95% confidence intervals.

Discussion

We have monitored the dynamic behavior of exocyst subunits fused to GFP by measuring fluorescence recovery from photobleaching at bud tips. We were able to divide exocyst subunits into two groups based on several criteria. The first group consists of Sec5p, Sec6p, Sec8p, Sec10p, Sec15p, and Exo84p, which all recovered with τ near to that of the vesicle-associated Rab GTPase, Sec4p. Their τ ranged from 11 s for Exo84p to 26 s for Sec6p, with an average of 18 s, compared with 12 s for Sec4p. Sec3p and Exo70p define the second group, which recovered severalfold more slowly. A key distinction between the two groups is their recovery behavior in the presence of Latrunculin A. Both Sec3p and Exo70p recovered in the presence of Latrunculin A, whereas the members of the first group all failed to do so. Therefore, the first group is distinguished from Sec3p and Exo70p not only by the speed with which they recover, but also by their requirement for an intact actin cytoskeleton for their recovery from photobleaching. This distinction from Sec3p is also evident in the results from immunoelectron microscopy and in vivo video microscopy. These experiments were designed to detect association of exocyst components with vesicles, and, in both cases, all subunits except for Sec3p were found to be in association with vesicles and moving in a manner consistent with vesicular traffic. The conclusion that we draw from these data is that all exocyst subunits, except for Sec3p, are transported to sites of exocytosis on vesicles, where they interact with Sec3p to tether those vesicles to the plasma membrane.

Exo70p can apparently use two distinct pathways to arrive at the bud tip, as seen by the biphasic nature of photobleaching recovery graphs. Supporting this possibility, Exo70p-GFP was found to maintain its localization in the presence of 200 μM Latrunculin A, which blocks vesicle delivery. Additionally, the fre-

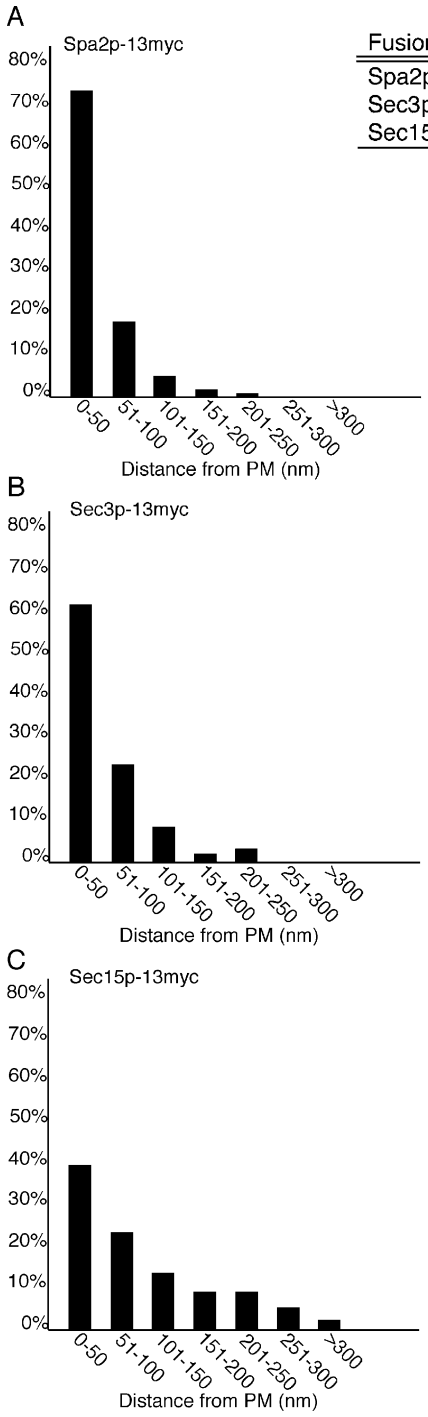

Fusion	D(nm)	s.d.	n(cells)	n(particles)
Spa2p-13myc	55.0	± 5.7	10	217
Sec3p-13myc	58.7	± 13.8	31	87
Sec15p-13myc	119	± 17.0	33	132

Figure 5. **Distribution of gold particles after immunoelectron microscopy.** Gold particles that were found to be in the bud tips of cells were counted, and the distances between all such particles and the plasma membrane were calculated. (A) Histogram showing the distribution of gold particle labeling when Spa2p-13myc was used as a negative control for vesicle association. Approximately 74% of the particles were found within 50 nm of the plasma membrane. Average distance between the plasma membrane and particles was found to be 55.0 ± 5.7 nm. (B) Histogram of the distribution of gold particles in a strain harboring the Sec3p-13myc fusion. 62% of gold particles were found to be within 50 nm of the plasma membrane, indicating that the majority of Sec3p-13myc was associated with the plasma membrane. Average distance between the plasma membrane and gold particles was 58.7 ± 13.8 nm. (C) Histogram of plasma membrane-gold particle distances in the Sec15p-13myc strain after immunoelectron microscopy. Less than half of the signal, 40%, was within 50 nm of the plasma membrane. These presumably represent Sec15p-13myc fusion proteins that are actively engaged in tethering vesicles to the plasma membrane in preparation for membrane fusion. The average distance from the plasma membrane to gold particles in the tip was found to be 119 ± 17 nm.

quency of full recovery from photobleaching for Exo70p-GFP was reduced in the presence of Latrunculin A, but not abolished (Fig. 3 C). In fact, the frequency of recovery in the presence of Latrunculin was similar to that for Sec3p-GFP in Latrunculin A, whereas when Latrunculin A was absent it was greater than that of Sec3p-GFP. The rate of recovery from photobleaching for Exo70p in the presence of Latrunculin ($\tau = 57 \pm 17$ s) was almost identical to the rate determined for Sec3p-GFP in both Latrunculin-treated and untreated cells ($\tau = 59 \pm 11$ s) and equivalent to the slow rate of Exo70p recovery as determined by analysis of photobleaching recovery curves generated in the absence of Latrunculin A. Finally, the association of Exo70p-13myc with vesicles in transit was shown by both immunoelectron microscopy and by video microscopy of cells harboring a triple-GFP tag fused to the COOH terminus of Exo70p. Our conclusion is that a portion of Exo70p is transported to sites of exocytosis on vesicles, possibly as part of a partially assembled exocyst complex, but approximately half also localizes independently of vesicle traffic through direct association with Rho proteins (Adamo et al., 1999; Robinson et al., 1999). In this case, it may be responsible for the Sec3p-independent route of exocyst localization that has previously been reported (Guo et al., 2001).

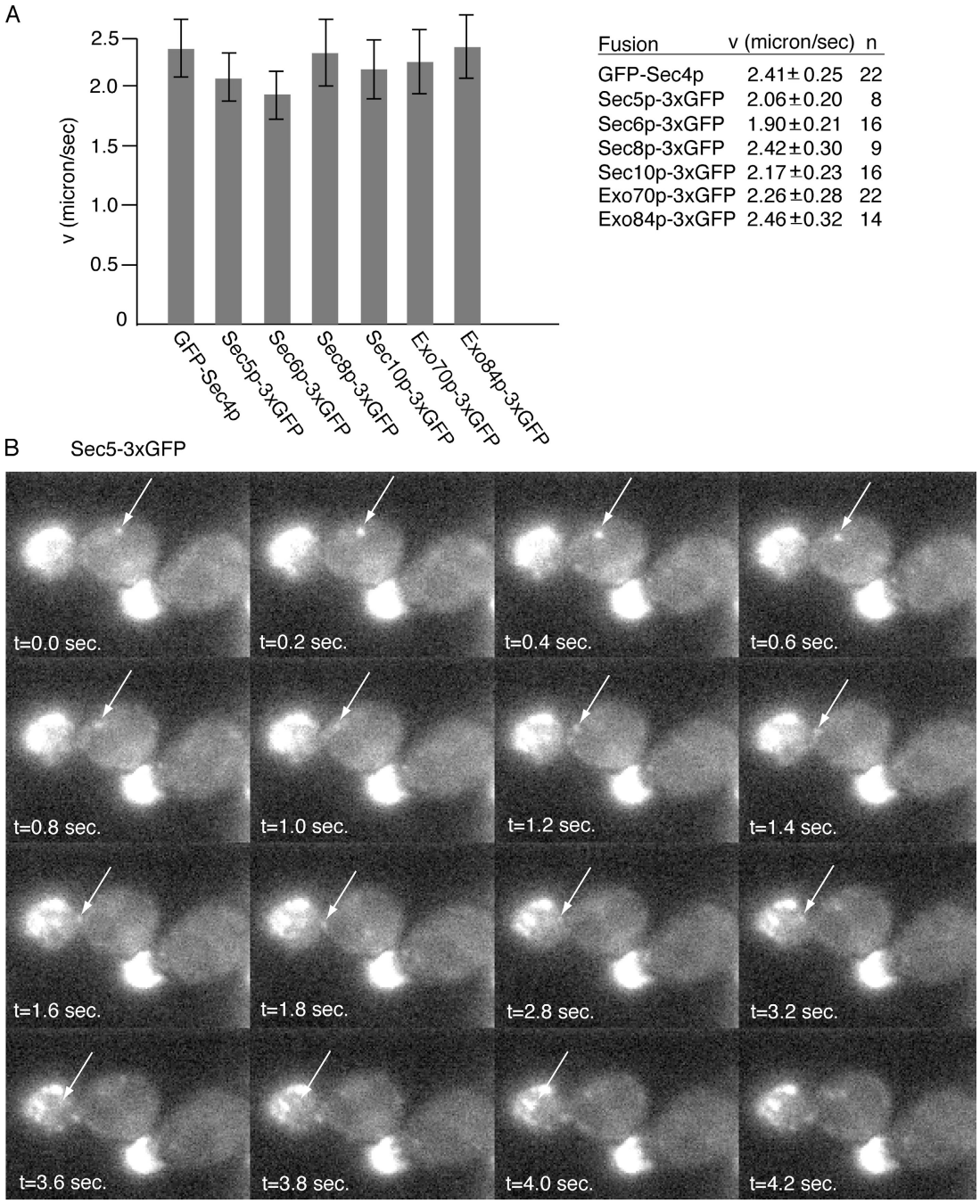

Fusion	v (micron/sec)	n
GFP-Sec4p	2.41± 0.25	22
Sec5p-3xGFP	2.06±0.20	8
Sec6p-3xGFP	1.90±0.21	16
Sec8p-3xGFP	2.42±0.30	9
Sec10p-3xGFP	2.17±0.23	16
Exo70p-3xGFP	2.26±0.28	22
Exo84p-3xGFP	2.46±0.32	14

Figure 6. **Videomicrography of exocyst subunits fused to triple GFP tags.** Haploid cells containing fusions of exocyst subunits to triple GFP tags were grown in SC medium and prepared for viewing as described in Materials and methods. Movies of 50 to 100 frames captured at five frames per second were analyzed for moving puncta consistent with vesicles in transit along actin cables. The velocity of individual puncta was calculated by determining the number of pixels traveled in a given number of frames and converting to micrometers per second. (A) Average speed of movement of puncta was determined for exocyst subunits fused to a triple-GFP tag as well as for GFP-Sec4p. We did not count movement near the mother-bud neck because movement rates there tend to be reduced as vesicles transition from the mother to the daughter cell. We did not calculate movement rates for Sec3p-3xGFP, which had no visible puncta movement, or Sec15p-3xGFP, which had puncta that were too faint to reliably track. Error bars represent 95% confidence intervals. (B) Videomicrographs of strain NY2510 containing exocyst subunit Sec5p fused to a 3xGFP tag. Capture rate is five frames per second. Contrast has been enhanced to visualize puncta. Several frames are shown here, with arrows indicating a punctum that travels from a mid-mother cell location near the upper shoulder into the bud tip during the course of about 4 s of video capture. Several frames captured during the time the punctum paused near the mother-bud neck were excised from the series. Quicktime videos of this movie and movies of all other visible subunits fused to 3xGFP are available in the online supplemental material (available at http://www/jcb.org/cgi/content/full/jcb.200408124/DC1).

In total, our data support a model in which a subset of subunits is delivered on vesicles and exocyst assembly is completed only as the vesicles arrive at sites of exocytosis marked by the remaining subunits, Sec3p and Exo70p (Fig. 8). An important implication of this model is that there must be a cycle of assembly for the exocyst. If we consider the cycle to begin with exocyst assembly and vesicle tethering, then a mechanism must exist for disassembly and recycling of the exocyst

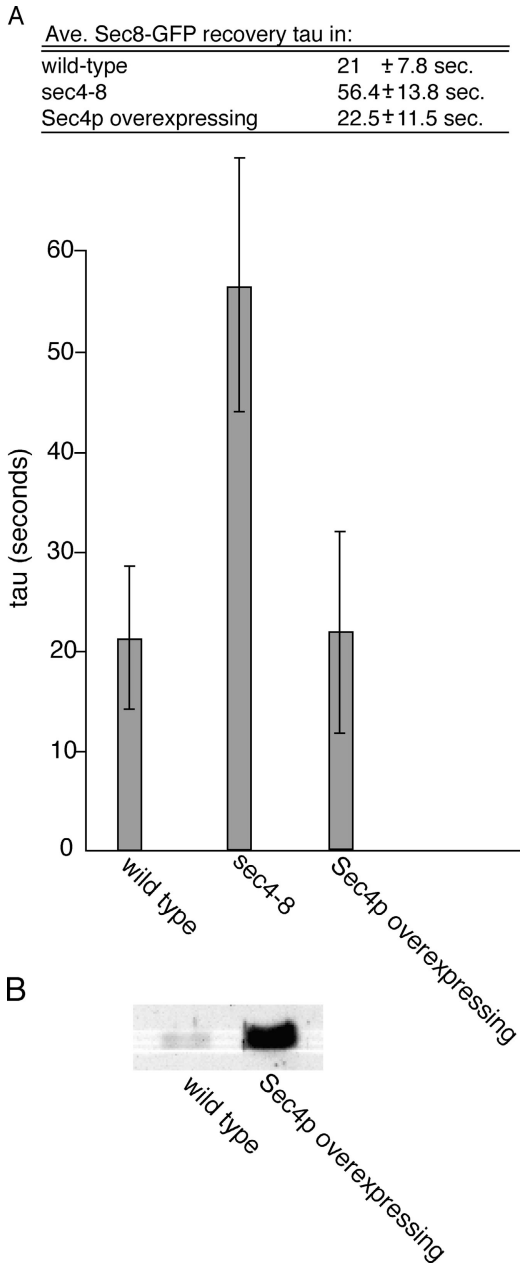

Figure 7. **Photobleaching recovery experiments on strains containing a Sec8p-GFP fusion protein with various alleles of *sec4*.** (A) Photobleaching recovery rates. Recovery from photobleaching in strain NY2443, which harbors Sec8p-GFP and the wild-type *SEC4* allele, had a τ of 23 $\pm$ 4.5 s. Compared with the wild-type background, recovery of the Sec8-GFP fusion was much slower in a strain harboring the *sec4-8* allele (NY2518), which had a recovery τ of 56 $\pm$ 14 s. Photobleaching recovery was measured in NY2518 at RT, substantially below the restrictive temperature of 30°C. Strain NY2519, which expresses approximately fivefold more Sec4p than NY2443, was also examined and found to have a τ of 22.5 $\pm$ 11.5 s. Error bars represent 95% confidence intervals. (B) Western blot of whole-cell extracts from strains NY1210 (wild type) and NY2520 (otherwise wild-type that contains the integrating Sec4p overexpression vector pNB170), showing that Sec4p is overproduced approximately fivefold in NY2520.

subunits (apart from Sec3p). We presently have no information on the mechanisms of disassembly and recycling. There must also be a mechanism for recruiting certain members of the exocyst onto newly formed, or forming, secretory vesicles. It has been speculated that exocyst components are loaded onto vesicles at the trans-Golgi (Munro, 2004), but this has yet to be shown experimentally.

Sec6p and Sec8p occupy intermediate positions with respect to some of the criteria that we have used to characterize exocyst components in this work. They have photobleaching recovery times that are somewhat longer than those for other actin-dependent exocyst subunits, and their association with vesicles as measured by immunoelectron microscopy is less robust than that for any other subunit except for Sec3p. But they both require actin for photobleaching recovery, and both are seen by videomicrography to move in a manner consistent with vesicular transport to sites of exocytosis. Why they should have photobleaching recovery times that are significantly greater than that for other exocyst subunits is unclear, but it may reflect a tendency to associate more strongly than other subunits with sites of exocytosis after tethering. With respect to the immunoelectron microscopy results, it may simply be the case that the tags are not readily accessible to the antibodies used to probe their locations in the cell. If the carboxy termini (and thus the 13myc tags) of Sec6p and Sec8p are less accessible than the carboxy termini of other subunits, then the detecting antibody would be less likely to bind the tag and this may well manifest itself as a reduced ratio of vesicle-specific labeling.

We have shown that the rate of recovery from photobleaching of a Sec8p-GFP fusion is dramatically reduced in a strain harboring the *sec4-8* allele. We feel that this result validates the use of FRAP as a diagnostic tool for investigating the affects of mutations on subunit dynamics, and provides evidence that the affect on recovery rates caused by Latrunculin A treatment are accurately representing changes in vesicle movement rates and are not due to secondary effects of depolymerizing actin. Although it is not surprising that loss of Sec4p function would alter the rate of recovery, it will be interesting to see how that effect is mediated. Does the *sec4-8* mutant fail to load exocyst subunits on secretory vesicles? Or, does Myo2p bind less effectively to vesicles in the *sec4-8* mutant, leading to a delay in delivery? A more thorough analysis of how Sec4p affects photobleaching recovery rates may help answer questions concerning the role of Rab GTPases in vesicle generation, association with motor proteins, and tethering.

Although Sec3p is the most stable member of the exocyst, the rate of recovery from photobleaching for the Sec3p-GFP fusion (τ = 59 $\pm$ 11 s) indicates that a rapid remodeling capability is maintained throughout the cell cycle. This finding is consistent with the requirement for dramatic remodeling of the exocytic machinery seen at two points in the cell cycle. The first transition is from a small region in the bud tip to an isotropic distribution in the large bud, and the second occurs when secretion moves from the bud surface to a ring around the mother-bud neck near the time of cytokinesis. Each of these transitions occurs in only a few minutes, so if Sec3p were substantially less dynamic, remodeling would be affected.

Secretory vesicles are targeted to sites of exocytosis in several distinct steps. Vesicles are transported along actin cables by the type V myosin, Myo2p (Govindan et al., 1995; Pruyne et al., 1998; Karpova et al., 2000). We have shown that

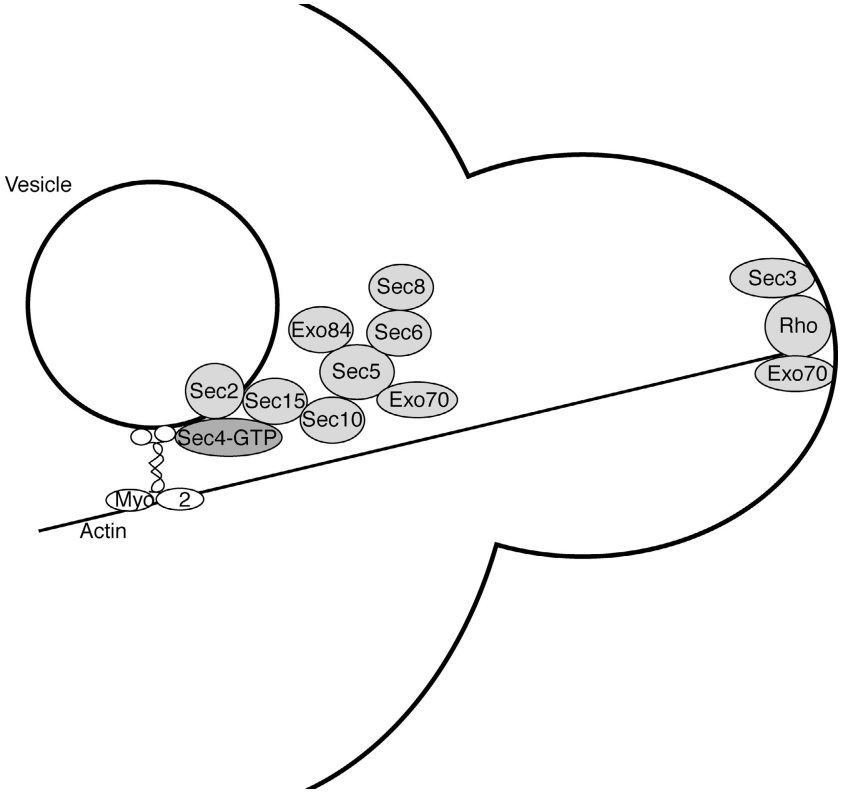

Figure 8. **Model of targeting and tethering in *S. cerevisiae*.** The exocyst subunits (except for Sec3p) associate with vesicles before movement to the bud tip. Once the vesicle has arrived at the bud tip, Sec3p and Exo70p bind to the rest of the exocyst to complete the formation of the tethering complex. Exo70p is also found to ride vesicles to sites of exocytosis in addition to localizing there by interacting with Rho3p.

most of the exocyst subunits are associated with the vesicles as they are transported. Once vesicles reach the end of the actin cable, they are tethered at sites of exocytosis through the interaction of the vesicle-associated exocyst subunits with Sec3p and Exo70p on the plasma membrane. Rho proteins coordinate vesicle delivery with vesicle tethering by interacting with both the formins, which assemble actin cables (Dong et al., 2003), as well as with Sec3p (Guo et al., 2001) and Exo70p (Adamo et al., 1999; Robinson et al., 1999), which mediate tethering. Assembly of the exocyst may serve to tether vesicles to tightly focused sites in preparation for membrane fusion, a step catalyzed by SNARE complexes. A key event of molecular recognition between target membrane and vesicles is initiated by the exocyst before SNARE complex assembly.

Materials and methods

Strain construction

Strains (constructed by J. Coleman, Yale University, New Haven, CT, and A. Grant, Centers for Disease Control, Atlanta, GA) harboring fusions to GFP were made by integrating fusion genes into the chromosomal locus of the particular gene to be fused to GFP. In the case of the GFP-SEC4 fusion, a GFP fusion vector based on pRS306 (Sikorski and Hieter, 1989) containing the GFP open reading frame cloned into the BamHI and NotI sites of the polylinker was used. For all remaining GFP fusions, integration constructs were made by PCR-mediated gene fusion with GFP and ligation into pPG5, a version of pRS306 that also contained the ADH1 downstream transcriptional termination region. Fusions of exocyst proteins to 13myc tags were accomplished by PCR-mediated gene replacement (Longtine et al., 1998). Fusions of exocyst proteins to 3xGFP (provided by B. Glick, University of Chicago, Chicago, IL) tags were accomplished by amplifying and cloning the COOH-terminal 1,000 base pairs into plasmid pPG5-3xGFP followed by digestion with appropriate enzymes and transformation. See Table II for a list of strains used in experiments and Table III for vectors and enzymes used in strain construction.

FRAP studies

FRAP experiments were conducted on *Saccharomyces cerevisiae* strains containing members of the exocyst fused at their COOH termini to GFP and on Sec4p fused at its NH_2 terminus to GFP. All the exocyst-GFP fusions were integrated into the chromosomal locus of the relevant exocyst subunit gene, and so were under the control of the normal promoter, and were the sole complete copies of the gene in the cell. All experiments were conducted on haploid cells. Cells were grown overnight in SC medium (Guthrie and Fink, 1991), diluted in the morning to OD = 0.2 and grown to OD = 1.0, all at 25°C. Approximately 1 ml of cells was pelleted and resuspended in 50 μl of fresh SC medium, and then 5 μl of this suspension was immobilized by mixing with an equal volume of 2% LMP agarose in PBS that had been melted and allowed to cool to 37°C. The cells and agarose were placed on a warm microscope slide, covered with a coverslip, and used in FRAP experiments. Bleaching and observation were conducted on an Axiovert inverted wide-field microscope (Carl Zeiss MicroImaging, Inc.) using Plan Neofluor apochromatic oil immersion 63× 1.3 NA objective lens, with fluorescence illumination provided by a 100-W xenon arc lamp. All bleaching and image acquisition was done at RT, ~22°C. The laser used in bleaching was a fixed-position dye-tunable laser emitting 3 mW at 440 nm, focused to a diffraction-limited spot ~1.0 μm in diameter. Recovery images were captured with either a MicroMax (Princeton Instruments) or a Retiga 1350EX cooled-CCD camera under the control of Scanalytics IPLab software, and best-fit bleaching and recovery curves were determined using IGOR statistical analysis program (WaveMetrics, Inc.). In some experiments, Latrunculin A (Molecular Probes; 10 mM in DMSO) was added to a concentration of 200 μM to determine recovery efficiency in the absence of actin cables.

To establish how many modes of action were contributing to recovery for each subunit, we manipulated the basic equation that describes recovery (Salmon et al., 1984):

$$I_\infty - I_t = (I_\infty - I_0)e^{-kt}, \quad (1)$$

where I_∞ is the signal intensity at full recovery, I_t is the signal intensity at time t, and I_0 is the signal intensity immediately after photobleaching. Rearranging this equation to

$$(I_\infty - I_t)/(I_\infty - I_0) = e^{-kt} \quad (2)$$

Table II. **Strains used**

Strain	Genotype
NY1210	Mat a GAL+ *ura3-52 leu2-3,112 his3Δ200*
NY2440	Mat a GAL+ *ura3-52 leu2-3,112 his3Δ200* SEC3-GFP (URA3)
NY2441	Mat a GAL+ *ura3-52 leu2-3,112 his3Δ200* SEC5-GFP (URA3)
NY2442	Mat a GAL+ *ura3-52 leu2-3,112 his3Δ200* SEC6-GFP (URA3)
NY2443	Mat a GAL+ *ura3-52 leu2-3,112 his3Δ200* SEC8-GFP (URA3)
NY2444	Mat a GAL+ *ura3-52 leu2-3,112 his3Δ200* SEC10-GFP (URA3)
NY2445	Mat a GAL+ *ura3-52 leu2-3,112 his3Δ200* SEC15-GFP (URA3)
NY2446	Mat a GAL+ *ura3-52 leu2-3,112 his3Δ200* EXO70-GFP (URA3)
NY2447	Mat a GAL+ *ura3-52 leu2-3,112 his3Δ200* EXO84-GFP (URA3)
NY2499	Mat a GAL+ *ura3-52 leu2-3,112 his3Δ200* SEC2-13myc (HIS3)
NY2500	Mat a GAL+ *ura3-52 leu2-3,112 his3Δ200* SEC3-13myc (HIS3)
NY2501	Mat a GAL+ *ura3-52 leu2-3,112 his3Δ200* SEC5-13myc (HIS3)
NY2502	Mat a GAL+ *ura3-52 leu2-3,112 his3Δ200* SEC6-13myc (HIS3)
NY2503	Mat a GAL+ *ura3-52 leu2-3,112 his3Δ200* SEC8-13myc (HIS3)
NY2504	Mat a GAL+ *ura3-52 leu2-3,112 his3Δ200* SEC10-13myc (HIS3)
NY2505	Mat a GAL+ *ura3-52 leu2-3,112 his3Δ200* SEC15-13myc (HIS3)
NY2506	Mat a GAL+ *ura3-52 leu2-3,112 his3Δ200* EXO70-13myc (HIS3)
NY2507	Mat a GAL+ *ura3-52 leu2-3,112 his3Δ200* EXO84-13myc (HIS3)
NY2508	Mat a GAL+ *ura3-52 leu2-3,112 his3Δ200* SPA2-13myc (HIS3)
NY2509	Mat a GAL+ *ura3-52 leu2-3,112 his3Δ200* SEC3-3xGFP (URA3)
NY2510	Mat a GAL+ *ura3-52 leu2-3,112 his3Δ200* SEC5-3xGFP (URA3)
NY2511	Mat a GAL+ *ura3-52 leu2-3,112 his3Δ200* SEC6-3xGFP (URA3)
NY2512	Mat a GAL+ *ura3-52 leu2-3,112 his3Δ200* SEC8-3xGFP (URA3)
NY2513	Mat a GAL+ *ura3-52 leu2-3,112 his3Δ200* SEC10-3xGFP (URA3)
NY2514	Mat a GAL+ *ura3-52 leu2-3,112 his3Δ200* SEC15-3xGFP (URA3)
NY2515	Mat a GAL+ *ura3-52 leu2-3,112 his3Δ200* EXO70-3xGFP (URA3)
NY2516	Mat a GAL+ *ura3-52 leu2-3,112 his3Δ200* EXO84-3xGFP (URA3)
NY2517	Mat a GAL+ *ura3-52 leu2-3,112 his3Δ200* GFP-SEC4 (URA3)
NY2518	Mat a GAL+ *ura3-52 leu2-3,112 his3Δ200* SEC8-GFP (URA3)
NY2519	Mat a GAL+ *ura3-52 leu2-3,112 his3Δ200* SEC8-GFP(LEU2) pNB170

Table III. **Fusion vectors used**

Strain	GFP fusion	13myc fusion	3xGFP fusion	Hemizap enzyme
Sec2	NA	Longtine et al., 1998	NA	NA
Sec3	pPG5	Longtine et al., 1998	pPG5-3xGFP	BstE II
Sec4	pRS306	NA	NA	NA
Sec5	pPG5	Longtine et al., 1998	pPG5-3xGFP	Bgl II
Sec6	pPG5	Longtine et al., 1998	pPG5-3xGFP	Afl II
Sec8	pPG5	Longtine et al., 1998	pPG5-3xGFP	PflM I
Sec10	pPG5	Longtine et al., 1998	pPG5-3xGFP	BsaB I
Sec15	pPG5	Longtine et al., 1998	pPG5-3xGFP	SexA I
Exo70	pPG5	Longtine et al., 1998	pPG5-3xGFP	BstE II
Exo84	pPG5	Longtine et al., 1998	pPG5-3xGFP	Bgl II
Spa2	NA	Longtine et al., 1998	NA	NA

and taking the natural logarithm of both sides and plotting the result against time will yield a straight line when only one factor is contributing to recovery, but a discontinuous line with two slopes when there are two factors that contribute.

Fluorescence and video microscopy

Epifluorescence microscopy and video microscopy of strains harboring exocyst proteins fused to a triple-GFP tag were conducted on cells grown overnight in SC medium at 25°C, and then diluted to OD = 0.2 and allowed to recover in fresh SC medium for 2 h at 25°C. Samples were collected by centrifugation, resuspended in fresh SC medium, and 7 μl of the suspension placed on a slide with coverslip. The cells were allowed to settle on the bottom surface of the slide for 5 to 10 min and examined on an Axioplan2 upright microscope (Carl Zeiss MicroImaging, Inc.) with 63× Plan Neofluor apochromatic oil-immersion objective lens with NA 1.3 and 100 W xenon excitation lamp. Images were captured with a cooled-CCD camera (model ORCA ER; Hamamatsu) and analyzed, and, if appropriate, enhanced with Openlab software (Improvision) running on an Apple G4 Macintosh computer. Still images were exposed for 0.25 to 1 s depending on sample brightness. Video images were collected with an exposure time of 160 ms per frame, resulting in a frame rate of five frames per second with no pixel binning. Individual movies varied in length from 50 to 100 frames (10 to 20 s).

EM

Strains analyzed by EM harbored a fusion of the relevant exocyst genes with 13 consecutive myc 9E10 epitopes, again as the sole copy and under the control of the wild-type promoter specific for the gene. Cells were grown overnight in SC medium, diluted in the morning to OD = 0.2 and grown to OD = 1.0, all at 25°C. Cells were fixed by addition of 37% formaldehyde to a concentration of 3.7% for 10 min, pelleted, resuspended in fixation medium (PBS + 2% glucose, 20 mM EGTA, and 3.7% formaldehyde), and incubated with shaking for 1 h at 25°C. Cells were washed twice in fixation medium without formaldehyde, resuspended in 250 mM Hepes, pH 7.4, with 8% PFA, and incubated overnight at 4°C without shaking. The fixed cells were pelleted and resuspended in 20% sucrose with 2% gelatin. After the gelatin had hardened, the gelatin cones were flash frozen in liquid nitrogen and thin cryo-sections were cut with a cooled ultramicrotome. Sections were incubated with commercial antibody against the 9E10 epitope (Invitrogen), labeled with 5- or 10-nm gold particles conjugated to protein A, and observed with an electron microscope (model 410; Philips). Images were captured at 16,500× on film (Kodak) and developed, and the negatives were examined to determine the surface area of cells and vesicles, as well as the number and distribution of gold particles compared with vesicles. Gold particles were considered to be associated with vesicles if they were within 50 nm of a subcellular structure unambiguously identifiable as a vesicle, as measured by examining negatives with a 7× loupe with submillimeter scale. However, if a gold particle was found to be within 50 nm of the plasma membrane, it was not counted as being associated with any vesicle. In this way, we eliminated association with the plasma membrane as a complicating factor when calculating vesicle-labeling ratio. The data yielded the cell area, the vesicle area (assuming an average vesicle radius of 40 nm), and the number of gold particles in each, and from these the density of gold particles in the cell as a whole (largely a function of washing efficiency) and the density of gold particles within 50 nm of a vesicle. We chose 50 nm as a conservative cutoff based on the size of the assembled mammalian exocyst (~30 to 35 nm; Hsu et al., 1998) and the lengths of the antibody (10 to 15 nm; Amit et al., 1985) and gold-conjugated protein A (5 to 10 nm).

Online supplemental material

Videos 1–7 show time-lapse movies, acquired at five frames per second and displayed at 25 frames per second, of otherwise wild-type cells (strain background NY1210) harboring GFP-Sec4p or exocyst subunits fused to a 3xGFP tag at their COOH termini. All videos were captured and processed as detailed in the Materials and methods section Fluorescence and video microscopy. Online supplemental material is available at http://www.jcb.org/cgi/content/full/jcb.200408124/DC1.

We thank Ben Glick for supplying the 3xGFP construct and Jeff Coleman and Althea Grant for strain construction.

C. Boyd was supported by National Institutes of Health (NIH) training grant DK0717-28. This work was supported by NIH grants GM35370 and CA 46128 awarded to P. Novick.

Submitted: 20 August 2004
Accepted: 19 October 2004

References

Adamo, J.E., G. Rossi, and P. Brennwald. 1999. The Rho GTPase Rho3 has a direct role in exocytosis that is distinct from its role in actin polarity. *Mol. Biol. Cell.* 10:4121–4133.

Amit, A.G., R.A. Mariuzza, S.E. Phillips, and R.J. Poljak. 1985. Three-dimensional structure of an antigen-antibody complex at 6 Å resolution. *Nature.* 313:156–158.

Andrews, H.K., Y.Q. Zhang, N. Trotta, and K. Broadie. 2002. *Drosophila* Sec10 is required for hormone secretion but not general exocytosis or neurotransmission. *Traffic.* 3:906–921.

Ayscough, K.R., J. Stryker, N. Pokala, M. Sander, P. Crews, and D. Drubin. 1997. High rates of actin filament turnover in budding yeast and roles for actin in establishment and maintenance of cell polarity revealed using the actin inhibitor latrunculin-A. *J. Cell Biol.* 137:399–416.

Bielinski, D.F., H.Y. Pyun, K. Linko-Stentz, I.G. Macara, and R.E. Fine. 1993. Ral and Rab3a are major GTP-binding proteins of axonal rapid transport and synaptic vesicles and do not redistribute following depolarization stimulated synaptosomal exocytosis. *Biochim. Biophys. Acta.* 1151:246–256.

Bowser, R., and P. Novick. 1991. Sec15 protein, an essential component of the exocytotic apparatus, is associated with the plasma membrane and with a soluble 19.5S particle. *J. Cell Biol.* 112:1117–1131.

Brymora, A., V.A. Valova, M.R. Larsen, B.D. Roufogalis, and P.J. Robinson. 2001. The brain exocyst complex interacts with RalA in a GFP-dependent manner: identification of a novel mammalian Sec3 gene and a second Sec15 gene. *J. Biol. Chem.* 276:29792–29797.

Conboy, M.J., and M.S. Cyert. 2000. Luv1p/Rki1p/Tcs3p/Vps54p, a yeast protein that localizes to the late Golgi and early endosome, is required for normal vacuolar morphology. *Mol. Biol. Cell.* 11:2429–2443.

Dong, Y., D. Pruyne, and A. Bretscher. 2003. Formin-dependent actin assembly is regulated by distinct modes of Rho signaling in yeast. *J. Cell Biol.* 161:1081–1092.

Drgonova, J., T. Drgon, D.H. Roh, and E. Cabib. 1999. The GTP-binding protein Rho1p is required for cell cycle progression and polarization of the yeast cell. *J. Cell Biol.* 146:373–387.

Drubin, D.G., and W.J. Nelson. 1996. Origins of cell polarity. *Cell.* 84:335–344.

Elias, M., E. Drdova, D. Ziak, B. Bavlnka, M. Hala, F. Cvrckova, H. Soukupova, and V. Zarsky. 2003. The exocyst complex in plants. *Cell Biol. Int.* 27:199–201.

Field, C., and R. Schekman. 1980. Localized secretion of acid phosphatase reflects the pattern of cell surface growth in *Saccharomyces cerevisiae*. *J. Cell Biol.* 86:123–128.

Finger, F.P., T.E. Hughes, and P. Novick. 1998. Sec3p is a spatial landmark for polarized secretion in budding yeast. *Cell.* 92:559–571.

Fujiwara, T., K. Tanaka, A. Mino, M. Kikyo, K. Takahashi, K. Shimizu, and Y. Takai. 1998. Rho1p-Bni1p-Spa2p interactions: implication in localization of Bni1p at the bud site and regulation of the actin cytoskeleton in *Saccharomyces cerevisiae*. *Mol. Biol. Cell.* 9:1221–1233.

Ghaemmaghami, S., W.K. Huh, K. Bower, R.W. Howson, A. Belle, N. Dephoure, E.K. O'Shea, and J.S. Weissman. 2003. Global analysis of protein expression in yeast. *Nature.* 425:737–741.

Goud, B., A. Salminen, N.C. Walworth, and P.J. Novick. 1988. A GTP-binding protein required for secretion rapidly associates with secretory vesicles and the plasma membrane in yeast. *Cell.* 53:753–768.

Govindan, B., R. Bowser, and P. Novick. 1995. The role of Myo2, a yeast class V myosin, in vesicular transport. *J. Cell Biol.* 128:1055–1068.

Grindstaff, K., C. Yeaman, N. Anandasabapathy, S.C. Hsu, E. Rodriguez-Boulan, R.H. Scheller, and W.J. Nelson. 1998. Sec6/8 complex is recruited to cell-cell contacts and specifies transport vesicle delivery to the basal-lateral membrane in epithelial cells. *Cell.* 93:731–740.

Guo, W., A. Grant, and P. Novick. 1999a. Exo84p is an exocyst protein essential for secretion. *J. Biol. Chem.* 274:23558–23564.

Guo, W., D. Roth, C. Walch-Salimena, and P. Novick. 1999b. The exocyst is an effector for Sec4p, targeting secretory vesicles to sites of exocytosis. *EMBO J.* 18:1071–1080.

Guo, W., F. Tamanoi, and P. Novick. 2001. Spatial regulation of the exocyst complex by Rho1 GTPase. *Nat. Cell Biol.* 3:353–360.

Guthrie, C., and G.R. Fink, eds. 1991. *Guide to yeast genetics and molecular biology.* Methods in Enzymology, vol. 194. San Diego: Academic Press.

Hsu, S.C., A.E. Ting, C.D. Hazuka, S. Davanger, J.W. Kenny, Y. Kee, and R.H. Scheller. 1996. The mammalian brain rsec6/8 complex. *Neuron.* 17: 1209–1219.

Hsu, S.C., C.D. Hazuka, R. Roth, D.L. Foletti, J. Heuser, and R.H. Scheller. 1998. Subunit composition, protein interactions, and structures of the mammalian brain sec6/8 complex and septin filaments. *Neuron.* 20: 1111–1122.

Karpova, T.S., S.L. Reck-Peterson, N.B. Elkind, M.S. Mooseker, P.J. Novick, and J.A. Cooper. 2000. Role of actin and Myo2p in polarized secretion and growth of *Saccharomyces cerevisiae*. *Mol. Biol. Cell.* 11:1727–1737.

Kim, D., M. Sacher, A. Scarpa, A.M. Quinn, and S. Ferro-Novick. 1999. High-copy suppressor analysis reveals a physical interaction between Sec34p and Sec35p, a protein implicated in vesicle docking. *Mol. Biol. Cell.* 10: 3317–3329.

Longtine, M.S., A. McKenzie III, D.J. Demarini, N.G. Shah, A. Wach, A. Brachat, P. Philippsen, and J.R. Pringle. 1998. Additional modules for versatile and economical PCR-based gene deletion and modification in *Saccharomyces cerevisiae*. *Yeast.* 14:953–961.

Moskalenko, S., D.O. Henry, C. Rosse, G. Mirey, J.H. Camonis, and M.A. White. 2002. The exocyst is a Ral effector complex. *Nat. Cell Biol.* 4:66–72.

Moskalenko, S., C. Tong, C. Rosse, G. Mirey, E. Formstecher, L. Daviet, J. Camonis, and M.A. White. 2003. Ral GTPases regulate exocyst assembly through dual subunit interactions. *J. Biol. Chem.* 278:51743–51748.

Munro, S. 2004. Organelle identity and the organization of membrane traffic. *Nat. Cell Biol.* 6:469–472.

Murthy, M., D. Garza, R. Scheller, and T. Schwarz. 2003. Mutations in the exocyst component Sec5 disrupt neuronal membrane traffic, but neurotransmitter release persists. *Neuron.* 37:433–447.

Nelson, W.J., and C. Yeaman. 2001. Protein trafficking in the exocytic pathway of polarized epithelial cells. *Trends Cell Biol.* 11:483–486.

Prigent, M., T. Dubois, G. Raposo, V. Derrien, D. Tenza, C. Rosse, J. Camonis, and P. Chavrier. 2003. ARF6 controls post-endocytic recycling through its downstream exocyst complex effector. *J. Cell Biol.* 163:1111–1121.

Pruyne, D.W., D. Schott, and A. Bretscher. 1998. Tropomyosin-containing actin cables direct the Myo2p-dependent polarized delivery of secretory vesicles in budding yeast. *J. Cell Biol.* 143:1931–1945.

Rieder, S.E., and S.D. Emr. 1997. A novel RING finger protein complex essential for a late step in protein transport to the yeast vacuole. *Mol. Biol. Cell.* 8:2307–2327.

Robinson, N.G., L. Guo, J. Imai, Y. Matsui, and F. Tamanoi. 1999. Rho3 of *Saccharomyces cerevisiae*, which regulates the actin cytoskeleton and exocytosis, is a GTPase which interacts with Myo2 and Exo70. *Mol. Cell. Biol.* 19:3580–3587.

Sacher, M., Y. Jiang, J. Barrowman, A. Scarpa, J. Burston, L. Zhang, D. Schieltz, J.R. Yates III, H. Abeliovich, and S. Ferro-Novick. 1998. TRAPP, a highly conserved novel complex on the cis-Golgi that mediates vesicle docking and fusion. *EMBO J.* 17:2494–2503.

Salmon, E.D., R.J. Leslie, W.M. Saxton, M.L. Karow, and J.R. McIntosh. 1984. Spindle microtubule dynamics in sea urchin embryos: analysis using a fluorescein-labeled tubulin and measurements of fluorescence redistribution after laser photobleaching. *J. Cell Biol.* 99:2165–2174.

Sans, N., K. Prybylowski, R.S. Petralia, K. Chiang, Y.-X. Wang, C. Racca, S. Vicini, and R.J. Wenthold. 2003. NMDA receptor trafficking through an interaction between PDZ proteins and the exocyst complex. *Nat. Cell Biol.* 5:520–530.

Schott, D., R. Collins, and A. Bretscher. 2002. Secretory vesicle transport velocity in living cells depends on the myosin-V lever arm length. *J. Cell Biol.* 156:35–39.

Sikorski, R.S., and P. Hieter. 1989. A system of shuttle vectors and yeast host strains designed for efficient manipulation of DNA in *Saccharomyces cerevisiae*. *Genetics.* 122:19–27.

Simonsen, A., R. Lippe, S. Christoforidis, J.M. Gaullier, A. Brech, J. Callaghan, B.H. Toh, C. Murphy, M. Zerial, and H. Stenmark. 1998. EEA1 links PI(3)K function to Rab5 regulation of endosome fusion. *Nature.* 394: 494–498.

TerBush, D.R., and P. Novick. 1995. Sec6, Sec8, and Sec15 are components of a multisubunit complex which localizes to small bud tips in *Saccharomyces cerevisiae*. *J. Cell Biol.* 130:299–312.

TerBush, D.R., T. Maurice, D. Roth, and P. Novick. 1996. The Exocyst is a multiprotein complex required for exocytosis in *Saccharomyces cerevisiae*. *EMBO J.* 15:6483–6494.

Walch-Solimena, C., R.N. Collins, and P.J. Novick. 1997. Sec2p mediates nucleotide exchange on Sec4p and is involved in polarized delivery of post-Golgi vesicles. *J. Cell Biol.* 137:1495–1509.

Walworth, N.C., B. Goud, A.K. Kacenell, and P. Novick. 1989. Mutational analysis of *SEC4* suggests a cyclical mechanism for the regulation of vesicular traffic. *EMBO J.* 8:1685–1693.

Whyte, J.R.C., and S. Munro. 2002. Vesicle tethering complexes in membrane traffic. *J. Cell Sci.* 115:2627–2637.

Wiederkehr, A., Y. Du, M. Pypaert, S. Ferro-Novick, and P. Novick. 2003. Sec3p is needed for the spatial regulation of secretion and for the inheritance of the cortical endoplasmic reticulum. *Mol. Biol. Cell.* 14:4770–4782.

Yeaman, C., K. Grindstaff, J. Wright, and W.J. Nelson. 2001. Sec6/8 complexes on trans-Golgi network and plasma membrane regulate late stages of exocytosis in mammalian cells. *J. Cell Biol.* 155:593–604.

Zhang, X., E. Bi, P. Novick, L. Du, K. Kozminski, J. Lipschutz, and W. Guo. 2001. Cdc42 interacts with the exocyst and regulates polarized secretion. *J. Biol. Chem.* 276:46745–46750.